Zero-diffusion domains in reaction-diffusion morphogenetic & epidemiologic processes

Jacques Demongeot, Jean Gaudart, Athanasios Lontos, Julie Mintsa, Emmanuel Promayon, Mustapha Rachdi

International Journal of Bifurcation and Chaos

Zero-diffusion domains in reaction-diffusion morphogenetic & epidemiologic processes

Jacques Demongeot*
TIMC-IMAG, UMR UJF-CNRS 5525, , AGIM [3] team, University J. Fourier of Grenoble, Faculty of Medicine, 38 700 La Tronche, France
Jacques.Demongeot@imag.fr

Jean Gaudart
LERTIM, EA 3283, Aix-Marseille University, Faculty of Medicine, 27 Bd Jean Moulin 13385 Marseille Cedex 5, France
Jean.Gaudart@univmed.fr

Athanasios Lontos, Julie Mintsa, Emmanuel Promayon and Mustapha Rachdi
TIMC-IMAG, UMR UPMF-CNRS 5525, AGIM [3] team, University P. Mendès-France of Grenoble, Faculty of Medicine, 38 700 La Tronche, France
Athanasios.Lontos@imag.fr, Julie.Mintsa@imag.fr, Emmanuel.Promayon@imag.fr and Mustapha.Rachdi@upmf-grenoble.fr

Received (to be inserted by publisher)

Classical models of morphogenesis by Murray and Meinhardt and of epidemics by Ross and McKendrick can be revisited in order to consider the colocalizations favoring interaction between morphogens and cells or between pathogens and hosts. The classical epidemic models suppose for example that the populations in interaction have a constant size and are spatially fixed during the epidemic waves, but the presently observed pandemics show that the long duration of their spread during months or years imposes to take into account the pathogens, hosts and vectors migration in epidemics, as well as the morphogens and cells diffusion in morphogenesis. That leads naturally to study the occurrence of complex spatio-temporal behaviors in dynamics of population sizes and also to consider preferential zones of interaction, i.e., the zero-diffusion sets, for respectively building anatomic frontiers and confining contagion domains. Three examples of application will be presented, the first proposing a model of Black Death spread in Europe (1348-1350), and the last ones related to two morphogenetic processes, feather morphogenesis in chicken and gastrulation in *Drosophila*.

Keywords: Morphogenesis modelling; epidemics modelling; zero-diffusion set; periodic solutions; population size dynamics; gastrulation; feather morphogenesis; Black-Death spread.

1. Introduction

Recent advances in morphogenesis and epidemics modelling have been obtained by introducing demographic aspects, i.e., by considering morphogen, cell, pathogen, host and vector populations whose global size

*Corresponding author.

changes during morphogenetic, epidemic and endemic histories, as well as spatial aspects about their diffusion, spread or genetic changes [Gaudart *et al.*, 2007, 2009, 2010; Glade *et al.*, 2007; Abbas *et al.*, 2009; Horie *et al.*, 2010]
In epidemic studies for example, the mathematical toolbox allowing these improvements has been introduced making classical models [Bernoulli, 1760; d'Alembert, 1761; Murray, 1763; L'épine, 1764; de Baux, 1766; May, 1770; Lambert, 1972; Trembley, 1796; Sprengel, 1815; Ross, 1916; McKendrick, 1925; Kermack & McKendrick, 1932, 1933; Mac Donald, 1957; Barry & Gualde, 2006] more realistic, hence more convenient for predicting and anticipating the spread, and also testing scenarios (like vaccination or any health policy limiting the contagion). As applications, one infectious disease dynamics, the Black Death spread during the middle age in Europe, and the dynamics of two important processes, feather morphogenesis in chicken and gastrulation in Drosophila, will be studied in the present paper.
Despite their simplicity, the models presented account qualitatively for the global shape of the endemic spatial distributions and of the morphogenetic patterns. Some perspectives will be drawn concerning the present epidemic risks: a model like that used for the Black Death spread retro-prediction would be, "mutatis mutandis", useful to predict the dynamical behavior of the future epidemics, by considering the population fluxes along the modern aerial routes, responsible of the rapid dissemination of the pathogenic agents and infectives in the present pandemics [Khan *et al.*, 2009].

2. Introduction to classical epidemiology: the Ross-McKendrick model

In the seminal work by D. Bernoulli [Bernoulli, 1760; Dietz & Heesterbeek, 2000, 2002; Zeeman, 1993] proposed for explaining the small pox dynamics, the population was divided into susceptibles (not yet been infected) and immunes (immunized for the rest of their life after one infection). In [Ross, 1916; McKendrick, 1925; Kermack & McKendrick, 1932, 1933] is proposed a more sophisticated model called Susceptible/Infective/Recovered with immunity (SIR) model, with equations (1):

$$\begin{aligned} \frac{dS}{dt} &= \delta S + \delta I + (\delta+\gamma)R - \beta SI - \delta S, \\ \frac{dI}{dt} &= \beta SI - (\nu+\delta)I, \\ \frac{dR}{dt} &= \nu I - (\delta+\gamma)R, \end{aligned} \tag{1}$$

where S (resp. I, R) denotes the size of Susceptible (Infective, Recovered) population with $S+I+R=N$, β (resp. δ, γ, ν) being the contagion (resp. death/birth, loss of resistance, immunization) rate. The epidemic parameter $R_0 = \beta N/(\nu+\delta)$ is the mean number of secondary infecteds by one primary infective and predicts, if it is greater than 1, the occurrence of an epidemic wave. By defining age classes S_i, I_i and R_i $(i=1,\ldots,n)$ in each subpopulation S, I and R, we have at any stationary state (S^*, I^*, R^*) the following relationships:

$$u^*(i) = \frac{S_i^*}{S_1^*}\ ,\ \nu^*(i) = \frac{I_i^*}{I_1^*}\ ,\ w^*(i) = \frac{R_i^*}{R_1^*} \tag{2}$$

where the probabilities for a newborn of being alive and either susceptible $u^*(i)$, infected $\nu^*(i)$ or immune $w^*(i)$ at age i make the link between the Bernoulli and the Ross-McKendrick models, but the weakness of the later still resides in many insufficiencies and approximations:

- when the population size of either susceptibles or infectives tends to be very large, the quadratic term SI has to be replaced by a Michaelian term $SI/[(k+S)(j+I)]$
- the immunized infectives or healthy carriers are neglected
- the total population size is supposed to be constant, the fecondity just equalling the natural mortality. The Bernoulli model taken implicitly into account the fecundity, and explicitly the natural mortality. The model by d'Alembert [d'Alembert, 1761] improved the Bernoulli's one by distinguishing the specific mortality due to the infectious disease from the natural one, being more widely applicable than the model by Bernoulli which was restricted to immunizing infections. d'Alembert's method needs the knowledge

about the survival function after eliminating the specific cause of death due to the infectious disease, but Bernoulli's approach provides more insight for a mechanistic interpretation of infection

- variables and parameters are not depending on space (no migration)
- parameters are not depending on time (no genetic adaptation of infectious agent or human population, even very slow compared to the fast dynamics of epidemics).

We will improve in the following the Ross-McKendrick model by trying to partially compensate these defects. We will first introduce the age classes into the host population in order to account for its growth, the space dependence in order to account for the host and vector population migration and their possible coexistence, before presenting an example of application and drawing perspectives. The genetic changes resulting from the adaptation of the concerned populations will be not treated in this paper.

3. Epidemics modelling with demography and diffusion

By exploiting the remarks formulated in the previous Section about the classical models of epidemic modelling, we now consider the possibility to merge the demographic dynamics introduced in [Demongeot, 2009] and the reaction-diffusion, by simplifying the von Foerster dynamics: we suppose that the biological age is identical to the chronological one and we choose for the host or vector populations dynamics the classical Fisher's equation [Fisher, 1937] with a logistic demographic term. We prove in the following that the asymptotic behavior of the spatial spread of the population size $n(s,t)$ over the spatial coordinates has a Gaussian shape. For the sake of simplicity, we consider the problem as isotropic and the space coordinate s as unidimensional.

Proposition 1. *Let us consider the Fisher-like equation defined by:*

$$\frac{\partial n}{\partial t} = \Delta n + n(K-n)^+ \text{ where } n(K-n)^+ = \begin{cases} n(K-n) & \text{if } n \leq K \\ 0 & \text{if } n > K \end{cases}$$

with the initial conditions: $n(.,0) = 1$. *Its asymptotic solution (t tending to infinity) is given by:*

$$n(s,t) = \exp\left(-\frac{s^2}{4t} + \ln(K) + \exp(-Kt)\right) t^{-1/2}$$

Proof. Let us suppose that $\dfrac{\partial n}{\partial t} = \Delta n + n(K-n)^+$. For $\frac{n}{K} \simeq 1$ (resp. $\frac{n}{K} \simeq 0$), we have:

$$n(K-n) \simeq -nK \ln\left(\frac{n}{K}\right) \quad (\text{resp. } \simeq nK)$$

Then, if we consider the solution n_1 of the heat operator, with $n_1(.,0) = 1$, and the solution n_2 of the logistic equation

$$\frac{\partial n_2}{\partial t} = -n_2 K \ln\left(\frac{n_2}{K}\right),$$

with $n_2(.,0) = 1$, we have:

(1) If $n_1(s,t) = \exp\left(-\dfrac{s^2}{4t}\right) t^{-1/2}$, then $\dfrac{\partial n_1}{\partial s} = -s\dfrac{n_1}{2t}$, hence

$$\Delta n_1 = \frac{\partial^2 n_1}{\partial s^2} = -\frac{n_1}{2t} + s^2 \frac{n_1}{4t^2} \text{ and } \frac{\partial n_1}{\partial t} = \left(\frac{s^2}{4t^2} - \frac{1}{2t}\right) n_1 = \Delta n_1$$

(2) If $\dfrac{n_2}{K} \simeq 1$ (resp. $\dfrac{n_2}{K} \simeq 0$), $n_2(s,t) = K\exp(\exp(-Kt))$ (resp. $n_2'(s,t) = \exp(Kt)$) is an approximate solution of

$$\frac{\partial n_2}{\partial t} = -n_2 K \ln\left(\frac{n_2}{K}\right) \text{ (resp. } \frac{\partial n_2'}{\partial t} = n_2' K)$$

Let us consider now $n = n_1 n_2$; we have:

$$\frac{\partial n}{\partial t} = \begin{cases} n_2 \dfrac{\partial n_1}{\partial t} + n_1 \dfrac{\partial n_2}{dt} = n_2 \Delta n_1 - n_1 n_2 K \ln\left(\dfrac{n_2}{K}\right), & \text{if } \dfrac{n_2}{K} \simeq 1 \\ n_2' \Delta n_1 - n_1 n_2' K, & \text{if } \dfrac{n_2}{K} \simeq 0 \end{cases}$$

Because n_2 (resp. n_2') is independent of s, then $n_2 \Delta n_1 = \Delta n$ (resp. $n_2' \Delta n_1 = \Delta n$) and we have:

$$n_1 n_2 K \ln\left(\frac{n_1}{K}\right) = K \exp\left(\exp(-Kt) - \frac{s^2}{4t}\right)\left[\frac{-s^2}{4t} - \frac{\ln(t)}{2} - \ln(K)\right] t^{-1/2}$$

tends to 0 when t tends to infinity, for every s.
It is the same for

$$n_1 n_2' K \ln\left(\frac{n_1}{K}\right) = \exp\left(Kt - \frac{s^2}{4t}\right)\left[-\frac{s^2}{4t} - \frac{\ln(t)}{2} - \ln(K)\right] t^{-1/2} \text{ when } t \text{ tends to 0.}$$

Then $n = n_1 n_2 = \exp\left(-\dfrac{s^2}{4t} + \ln(K) + \exp(-Kt)\right) t^{-1/2}$ is asymptotically in t the solution of the Fisher-like equation $\dfrac{\partial n}{\partial t} = \Delta n + n(K-n)^+$, $n = n_1 n_2'$ being the approximate solution when t is small.

■

If we consider that the diffusion and the demographic growth are slow compared to the fast epidemic dynamics, then the initial condition of the Fisher-like equations is the stable steady state of the reaction part of the system of equations (3), defined by:

$$\begin{aligned} \frac{\partial S}{\partial t} &= \Delta S + S(K_1 - S)^+ - \frac{bSI + k_1 S}{\varepsilon} \\ \frac{\partial I}{\partial t} &= \Delta I + I(K_2 - I)^+ + \frac{bSI - k_2 I}{\varepsilon} \end{aligned} \tag{3}$$

Proposition 2. *If we denote the fast endemic steady state of (3), supposed to be stable, by (S^*, I^*), then we have as asymptotic (in t) solution of (3) the Gaussian-like functions:*

$$S(s,t) = S^* \frac{\exp\left(-\frac{s^2}{4t} + \ln(K_1) + \exp(-K_1 t)\right) t^{-1/2}}{\exp\left(-\frac{s^2}{4t^*} + \ln(K_1) + \exp(-K_1 t^*)\right) t^{*-1/2}}$$

$$I(s,t) = I^* \frac{\exp\left(-\frac{s^2}{4t} + \ln(K_2) + \exp(-K_2 t)\right) t^{-1/2}}{\exp\left(-\frac{s^2}{4t^*} + \ln(K_2) + \exp(-K_2 t^*)\right) t^{*-1/2}}$$

for $t \geq t^*$, where t^* denotes the first time where $(S(s,t^*), I(s,t^*))$ approximates (S^*, I^*) with a precision equals to ε in Euclidean norm:

$$\left((S(s,t^*) - S^*)^2 + (I(s,t^*) - I^*)^2\right)^{1/2} = \varepsilon$$

Proof. The result is the direct consequence of the Proposition 1 and of the fastness of the epidemic dynamics. ■

There is an asymptotic identity between the zero-diffusion lines of the susceptibles and of the infecteds, if the asymptotic mode and variance of their Gaussian shaped functions are the same. When the contagion coefficient b is considered as depending on space, we choose $b(s)$ as maximal, equal to b^*, on zero-diffusion lines, i.e., where susceptibles and infecteds have the maximum of chance to coexist and we denote the steady state values of the fast epidemic dynamics (for b^*) as S^{**} and I^{**}. If there is no asymptotic identity, we can define $b(s)$ as inversely proportional to the distance between s and the zero-diffusion set located

around the concentration peaks.
Let us suppose now that the fast dynamics are the demographic and epidemic ones and that they are driven by the following differential equations:

$$\begin{aligned}\frac{dx}{dt} &= kx(N-x) - C\frac{xy}{(K+y)} - kk_1x \\ \frac{dy}{dt} &= fy + C\frac{xy}{(K+y)} - k_2y,\end{aligned} \tag{4}$$

where the host population growth (its size being represented by the variable x) is logistic, the fecundity being limited by a Malthusian term depending on the maximal population size N. The contagion interaction is supposed to have a Michaëlian saturation term [Crauste *et al.*, 2008] for controlling a possible excess of infective vectors (whose population size is y), and the mortality is assumed to be different between host and vector. By denoting $a = k(N-k_1)$ and $b = -f + k_2$, the system (4) becomes:

$$\begin{aligned}\frac{dx}{dt} &= -kx_2 - C\frac{xy}{(K+y)} + ax \\ \frac{dy}{dt} &= C\frac{xy}{(K+y)} - by\end{aligned} \tag{5}$$

Proposition 3. *The steady states of the system (5) are of three types:*

- *a stable node (resp. focus)* (x^*, y^*)*, in case of small mortality of infecteds* $(b \ll 1)$*, if*

$$a > 1 \text{ and } (C-a)(a-1) > 2kb \quad (\text{resp. } a < 1, 4(1-a)C > ab)$$

- *a stable node, in case of fast epidemics* $(C \gg K$ *and* $a = b = C)$*, if* $k \leq 1$.
- *a neutral steady state* $(x^{**}, y^{**}) = (0, 0)$.

Proof. The Jacobian matrix B^* of the system (5) at the steady state (x^*, y^*) is equal to:

$$B^* = \begin{pmatrix} -2kx^* - b\dfrac{y^*}{x^*} + a & -b\dfrac{K}{(K+y^*)} \\ b\dfrac{y^*}{x^*} & b\dfrac{K}{(K+y^*)} - b \end{pmatrix}$$

The non zero stationary state is defined by:

$$x^* = \frac{b}{C}(K+y^*) \text{ and } kx^{*2} + (C-a)x^* - bK = 0,$$

therefore the only positive solution, distinct from the saddle, is given by:

$$x^* = \frac{a - C + \left((a-C)^2 + 4bkK\right)^{1/2}}{2k},\ y^* = \frac{C}{b}x^* - K.$$

Therefore, the characteristic polynomial of the matrix $B^* - \lambda I$, denoted P_{B^*}, is equal to:

$$\begin{aligned}P_{B^*}(\lambda) = \lambda^2 + \left[2kx^* + b\frac{y^*}{x^*} + b - a - b\frac{K}{(K+y^*)}\right]\lambda + ab\frac{K}{(K+y^*)} \\ -ab - 2kx^*\left[b\frac{K}{(K+y^*)} - b\right] + b^2\frac{y^*}{x^*} = 0\end{aligned}$$

and, because

$$b^2\frac{K}{C} - \left(2kx^{*2} + (b-a)x^* + by^*\right) = bK\left(\frac{b}{C} - 1\right) - (a+b-C)x^*,$$

we have:

$$2x^*\lambda = bK\left(\frac{b}{C}-1\right)-(a+b-C)x^* \pm \left[\left(bK(\frac{b}{C}-1)-(a+b+C)x^*\right)^2 \right.$$
$$\left. +8kx^{*2}\left(b^2\frac{K}{C}-bx^*\right)-4b^2y^*x^*-4abx^*\left(b\frac{K}{C}-x^*\right)\right]^{1/2}.$$

We have also:

$$8kx^{*2}\left(b^2\frac{K}{C}-bx^*\right)-4b^2y^*x^*-4abx^*\left(b\frac{K}{C}-x^*\right)$$
$$=4bx^*\left[-2kx^{*2}+x^*\left(2bk\frac{K}{C}-C+a\right)-bK\left(\frac{a}{C}-1\right)\right]$$

and

$$2Cx^*\lambda = bK(b-C)-C(a+b-C)x^* \pm \left[[bK(b-C)-C(a+b-C)x^*]^2 \right.$$
$$\left. +4bCx^*\left[-2Ckx^{*2}+(2bkK+C(a-C))x^*-bK(a-C)\right]\right]^{1/2}.$$

Hence, we have:

(1) if $b \ll 1$ such as $bK/C-a \ll 1$, then we have:

$$x^* \simeq b\frac{K}{C-a}>0,\ y^* \simeq a\frac{K}{C-a}>0,\ bK\left(\frac{b}{C}-1\right)-(a+b-C)x^* \simeq -ab^2\frac{K}{C}(C-a)<0$$
$$\text{and } 8kx^{*2}\left(b^2\frac{K}{C}-bx^*\right)-4b^2y^*x^*-4abx^*\left(b\frac{K}{C}-x^*\right) \simeq -4ab\frac{K^2}{C(C-a)^2}\left(\frac{2bk}{C-a}+1-a\right)$$

(x^*,y^*) is a stable node ($a>1$ and $(C-a)(a-1)>2kb$) or focus ($a<1$ and $4a(1-a)b^3K^2>akb^4K^2/C$, i.e., $4(1-a)C>ab$). For example, if we choose $a=b=C/3=4K=1/3$ and $k=1$, then: $x^*=0.236/6$, $y^*=0.035$ and the B^* eigenvalues are given by:

$$\lambda=(-0.0054\pm[(0.0054)^2+0.052(-0.0031-0.0238+0.0093)]^{1/2})/0.472$$

and (x^*,y^*) is a stable focus.

(2) if $a=b=C \gg K$ and $k \leq 1$, then $x^*=(CK/k)^{1/2}, y^*=(CK/k)^{1/2}-K$ and the B^* eigenvalues are:

$$\lambda=\left[-\frac{C}{2}\pm\frac{C}{2}\left(1-8\left(\frac{Kk}{C}\right)^{1/2}\right)\left(1-\left(\frac{Kk}{C}\right)^{1/2}\right)\right]^{1/2}.$$

Then (x^*,y^*) is a stable node.

The Jacobian matrix B^{**} of the system (5) at the steady state (x^{**},y^{**}) is equal to:

$$B^{**}=\begin{pmatrix} a & -b \\ 0 & 0 \end{pmatrix}$$

Then (x^{**},y^{**}) is a neutral steady state. ■

Suppose that the contagion interaction has a double Michaëlian saturation term for controlling both a possible excess of susceptibles (whose population size is x) and of infective vectors (whose population size is y), then the system (5) becomes:

$$\frac{dx}{dt}=-kx^2-C\frac{xy}{(J+x)(K+y)}+ax \qquad (6)$$
$$\frac{dy}{dt}=C\frac{xy}{(J+x)(K+y)}-by$$

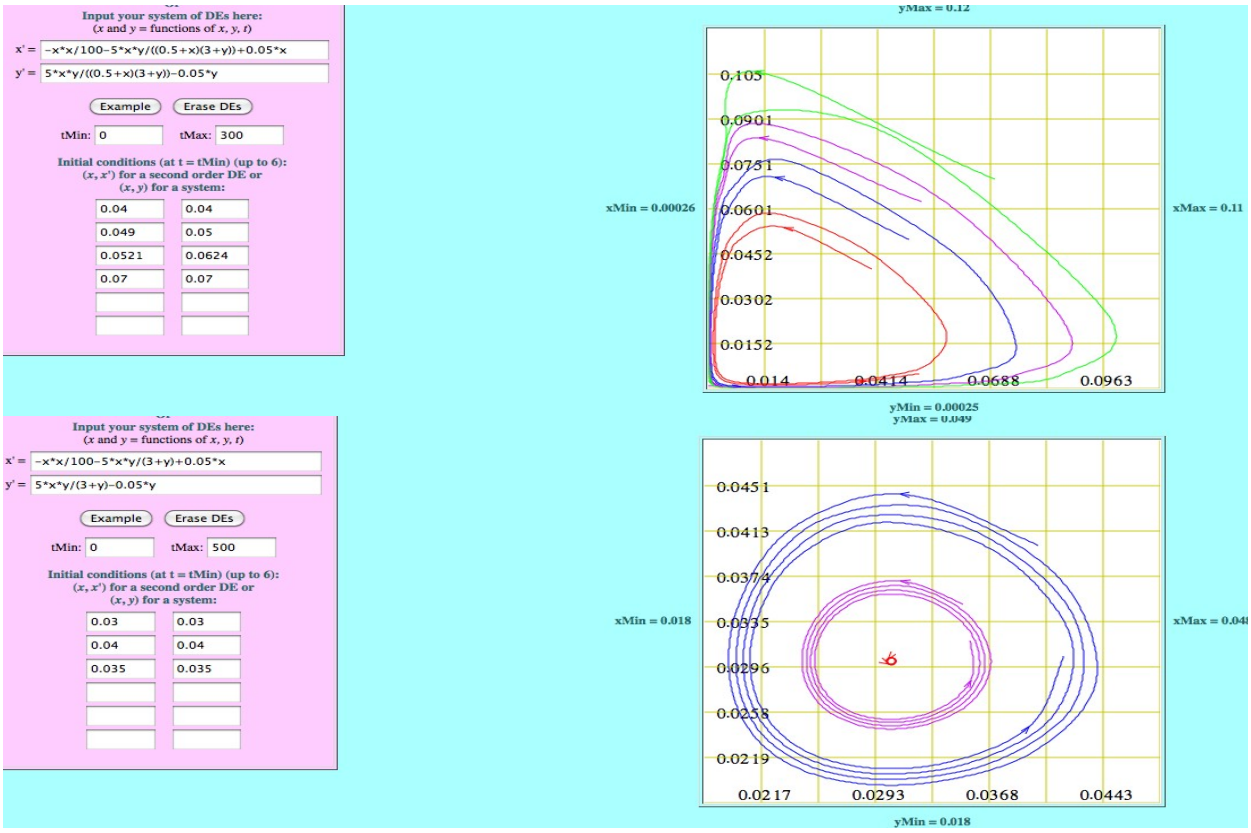

Fig. 1. Attractor of the system with double saturation (6) showing (top) a limit cycle and attractor of the system with a unique saturation term (5) showing (bottom) a stable focus for different initial conditions and for the same set of values of parameters in case (5) and (6) except for the affinity coefficient J (cf. for the numerical simulations the web site: http://www.zweigmedia.com/RealWorld/deSystemGrapher/func.html)

Proposition 4. *The steady states of the system (6) are of three types:*

- *a stable node (resp. focus)* (x^*, y^*)*, in case of large saturation of susceptibles* $(J \gg 1)$ *and of small mortality of infecteds* $(b \ll 1)$*, if*

$$a > 1 \text{ and } \left(\frac{C}{J} - a\right)(a-1) > 2kb \quad \left(\text{resp. } a < 1 \text{ and } 4(1-a)\frac{C}{J} > ab\right)$$

- *an unstable focus, in case of slow demographic dynamics* $(k \ll 1)$*, compared to the reaction* $(C > 3)$*, with* $a = b < 1/2K$ *and* $K > JC > 1$.
- *a neutral steady state* $(x^{**}, y^{**}) = (0, 0)$.

Proof. Let us prove the second assertion. If $k \ll 1$, the x^2 term is neglectible, and (x^*, y^*) verifies:

$$\frac{Cx^*y^*}{a(J+x^*)(K+y^*)} \simeq x^* \simeq y^*$$

hence

$Cx^* \simeq a(J+x^*)(K+Cx^*) = aJK + a(JC+K)x^* + aCx^{*2}$ and $aCx^{*2} + (aJC + aK - C)x^* + aJK = 0$.

Then, if we denote $-D = C - aJC - aK > 0$, we have:

$$D^2 - 4a^2CJK = (C + aJC - aK)^2 - 4aC^2J > (C - aK)^2 - 4aCK > (C - 0.5)^2 - 2C > 0$$

and

$$2aJK > x^* = \frac{-D - (D^2 - 4a^2CJK)^{1/2}}{2aC} > 0.$$

Then the eigenvalues λ of the Jacobian matrix B^* of the system (6) at the stationary point (x^*, y^*) are given by $det(B^* - \lambda I) = P_{B^*}(\lambda) = 0$, where:

$$B^* - \lambda I = \begin{pmatrix} -CJ\dfrac{y^*}{(J+x^*)^2(K+y^*)} + a - \lambda & -CK\dfrac{x^*}{(K+y^*)^2(J+x^*)} \\ CJ\dfrac{y^*}{(J+x^*)^2(K+y^*)} & CK\dfrac{x^*}{(K+y^*)^2(J+x^*)} - b - \lambda \end{pmatrix}$$
$$= \begin{pmatrix} a\dfrac{x^*}{J+x^*} - \lambda & -K\dfrac{b}{K+y^*} \\ J\dfrac{a}{J+x^*} & -b\dfrac{y^*}{K+y^*} - \lambda \end{pmatrix}$$

Hence, we have for the characteristic polynomial P_{B^*} of B^*:

$$P_{B^*}(\lambda) = \lambda^2 - \left[a\frac{x^*}{J+x^*} - b\frac{y^*}{K+y^*}\right]\lambda + ab\frac{KJ - x^*y^*}{(J+x^*)(K+y^*)}.$$

Then the eigenvalues λ are complex with a positive real part and gives birth to a limit cycle after a Hopf bifurcation (cf. Figure 1), because: $K > J$ implies

$$\frac{ax^*}{J+x^*} - \frac{by^*}{K+y^*} > 0$$

and since $x^* > 2aJK$ with $a < 1/(2K) < 1/(2J)$, we obtain:

$$\frac{4abKJ}{(J+x^*)(K+y^*)} = \frac{4a^3JK}{Cx^*} > \frac{4a^2C}{C^2} > \frac{a^2}{C^2}(aK + aJ + 2ax^*)^2 = \left(\frac{ax^*}{J+x^*} + \frac{by^*}{K+y^*}\right)^2.$$

The other results of the Proposition 4. are proved as in Proposition 3. ■

4. Definition of the biological age

By introducing a biological age a different from the chronological age t of the demographic dynamics [Demongeot, 2009], we replace the logistic term in equations (4), (5) and (6) by a von Foerster-like partial differential equation, where we denote by σ_x the biological age shift of an individual susceptible with respect to its chronological age t:

$$\sigma_x x_a(a,t) + x_t(a,t) = -\mu_x x(a,t), \tag{7}$$

where $x(a,t)$ is the number of susceptibles in biological age a at time t.
If an ageing acceleration γ_x of an individual with respect to its chronological age t is allowed, a generalized von Foerster's equation can be used [Demongeot, 2009]:

$$\sigma_x x_a(a,t) + \Box x + x_t(a,t) = -\mu_x x(a,t), \tag{8}$$

where the demographic d'Alembertian operator is equal to $\Box x = \gamma_x \partial^2 x/\partial a^2 - \Delta x$ and where μ_x is the natural mortality coefficient of the susceptibles. The values of parameters like σ_x, γ_x and μ_x can depend both on space, biological age and time.

5. Introduction of a spatial dynamics

The introduction of the space in Ross-McKendrick models can be done through stochastic spatial Markovian or renewal models [Demongeot & Fricot, 1986] or through deterministic Partial Differential Equations (PDE's) in which the diffusion of hosts or vectors is modelled by the Laplacian operator Δ or possibly by the d'Alembertian $\Box$, when some sub-populations can present an accelerated ageing [Demongeot, 2009].

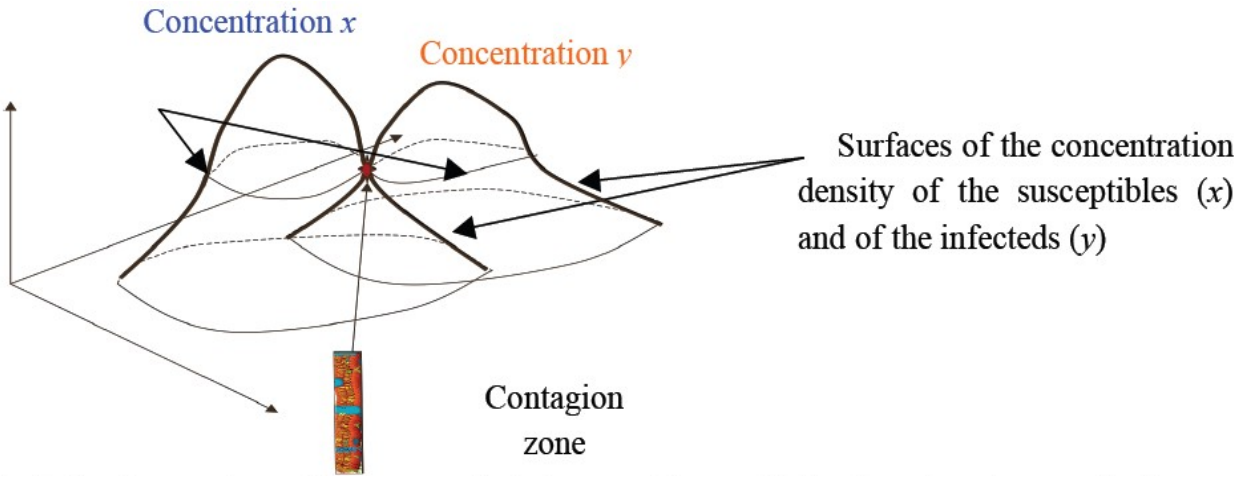

Fig. 2. Coexistence of zero-diffusion zones for both susceptibles x and infecteds y, where the contagion is maximum, in the case of an isotropic diffusion of these two populations

These models are called SIR with Diffusion ($SIRD$) [Gaudart *et al.*, 2010]. During the susceptible and infective vector spread, the maximum of contagion is observed on the common zones of least diffusion, which can be asymptotically identical, the common zero-diffusion domains allowing a maximum of contacts between interacting species (cf. Figure 2), i.e., reducing the effect of the thermic fluctuations which give birth to large values of the diffusion coefficients.
Taking into account the diffusion of all vector subpopulations (vector susceptibles, infecteds/non infectives and infectives), it is possible to simulate a model and compare its numerical results to the data recorded on the ground. For improving the fit, we take into account the diffusion of the human subpopulations S, G, I and R (susceptibles, infectives, infecteds/non infectives and recovereds). The contagion parameters are chosen depending on space, e.g., being maximum in zones where diffusion of infective vectors (A_i) and susceptible hosts (S) is minimum and in zones where sizes S of susceptible hosts and A_i of infective vectors are maximum ($D_S\,\Delta S/S$ minimum), ensuring locally a large coexistence time, i.e., a high contagion rate in interacting subpopulations. In case of isotropic diffusion, the zero-diffusion or zero Laplacian (or zero curvature or maximal gradient) lines of the concentration surfaces of the concerned populations are, if they are identical (cf. Figure 2), such a contagion domain, where hosts, vectors and infectious agents interact. These lines correspond to regions where the mean Gaussian curvature of the concentration surfaces S and A_i vanishes, these lines regions defined respectively by

$$\frac{\partial^2 S}{\partial x^2}\frac{\partial^2 S}{\partial y^2} - \left(\frac{\partial^2 S}{\partial x \partial y}\right)^2 = 0, \text{ and by } \frac{\partial^2 A_i}{\partial x^2}\frac{\partial^2 A_i}{\partial y^2} - \left(\frac{\partial^2 A_i}{\partial x \partial y}\right)^2 = 0.$$

We can show the possibility of intersection of these lines on one tangency point or on two points (cf. Figure 2) or on whole zero-diffusion sets if they are asymptotically identical (cf. Figure 6 bottom) for some values of the ratio between diffusion coefficients D_S/D_{A_i} [Michon *et al.*, 2008].

6. An example of application: the Black Death in Europe between 1348 and 1350

Plague was considered as endemic in the steppes of Southern-Russia where Mongols originated [Zhang *et al.*, 2008]. Born in the Caspian sea area (probably triggered by contacts between Mongolian and Genoa sailors and warriors during wars around 1346), epidemic wave went through the Mediterranean routes (cf. Figure 3). It reached ports like Marseilles in France and Genoa in Italy at the end of the year 1347. During 5

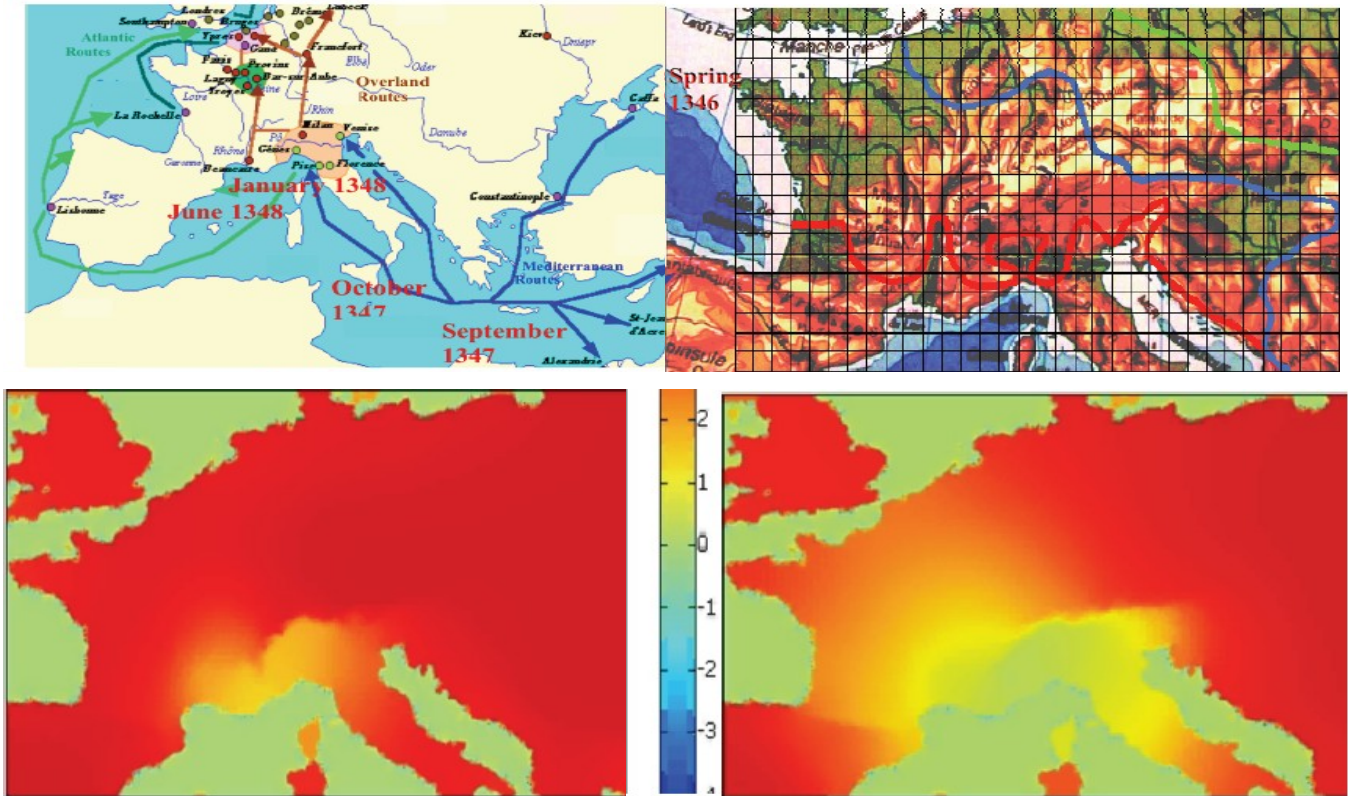

Fig. 3. Top left: spread of bubonic plague over see and overland routes (after <http://www.cosmovisions.com/ChronoPestesMA02.htm>). Top right: Observed wave fronts after 1 (red), 2 (blue) and 3 (green) years of spread from the two initial Mediterranean entry ports Genoa and Marseilles (1348) until the Atlantic ocean (1350) [Mocellin-Spicuzza, 2002]; black grid corresponds to the collected altitudes. Bottom: Simulation of equation (9) with wave fronts of concentration of susceptibles S after 3 (left) and 12 (right) months from Marseilles and Genoa

years it was spread widely in Europe from these two large commercial cities and come back to the Caspian reservoir. A simple Susceptible-Infective-Recovered model with Diffusion ($SIRD$) explains the essential of the observed front wave dynamics during years between 1348 and 1350 [Gaudart *et al.*, 2010]. The model uses only 3 coefficients: (i) a local viscosity proportional to the altitude, (ii) a contagion parameter and (iii) a death/recovering parameter (representing the future of infecteds/infectives as dead or immunized after being cured of the plague).

The Fisher equation [Fisher, 1937; Murray, 2003] has been firstly used for representing the evolution of the host and vector sub-populations during the spread of the Black Death.

The model used for modelling the Black Death spread is a $SIRD$ model as in the Bankoumana study [Gaudart *et al.*, 2007, 2009, 2010], but without vector terms and has for its reaction term the form of a Lotka-Volterra Ordinary Differential Equation (ODE) of dimension 3, plus a diffusion term:

$$\begin{aligned} \frac{dS}{dt} &= \varepsilon \Delta S - \beta SI, \\ \frac{dI}{dt} &= \varepsilon \Delta I + \beta SI - \gamma R, \\ \frac{dR}{dt} &= \varepsilon \Delta R + \gamma R, \end{aligned} \tag{9}$$

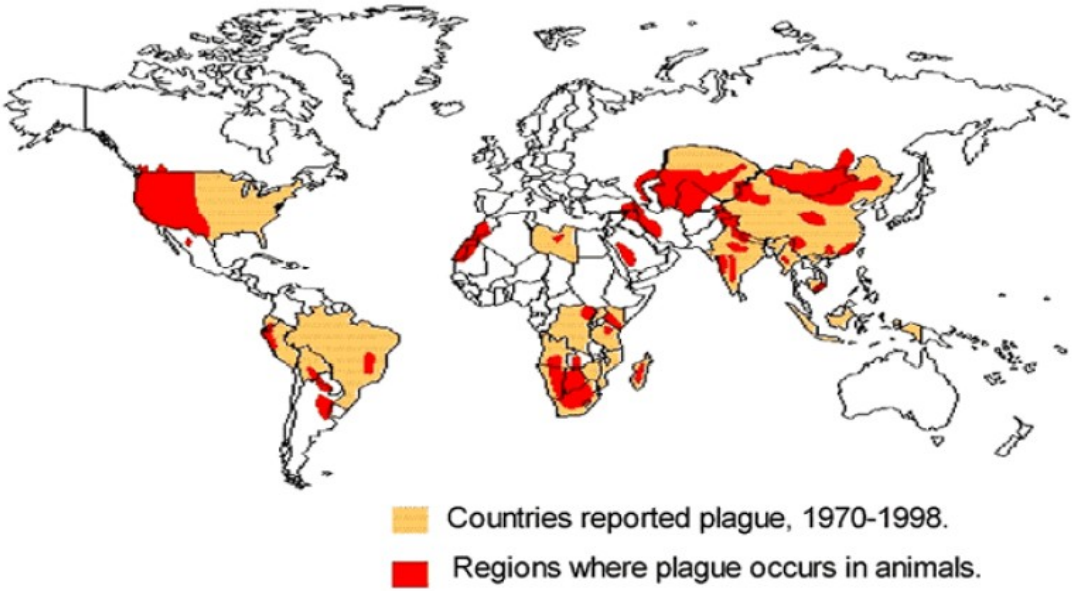

Fig. 4. World distribution of plague in 1998 (after [WHO, 1999])

where βSI term comes from the "law of mass action", assuming homogeneous mixing between susceptibles and infecteds, β being the rate of transition from susceptible to infected state calculated per infected and per susceptible, γ is the rate of transition from infected to post-infected state (e.g., death or immunity) per infected person and ε is the diffusion coefficient. By taking the viscosity (inverse of ε) proportional to the altitude, the simulated front waves are more similar to the observed ones (cf. Figure 3) than in the previous simulations [Murray, 2003]. The initial population size of susceptibles in the main middle age cities has been fixed following the demographic data. The results of simulations (cf. Figure 3 bottom) are in agreement with the data observed in the 370 hospitals of the order of St Anthony (cf. Figure 3 top right). Improvements could come from considering multiple entrance points (ports like Barcelona reached in June 1348 or La Rochelle, Rouen and Dover reached later in 1348), and taking into account all the commercial sea (Mediterranean and Atlantic) and overland routes (cf. Figure 3 top left) as well as the demography (fecundity and natural mortality). The present endemic state (cf. Figure 4) could be explained by a new model taking into account the air routes [WHO, 1999]. An efficient prediction from simulations of a realistic model taking into account new aerial routes with a minimal viscosity [Khan *et al.*, 2009] could serve this cause. Another improvement could come from considering saturation effects like those taken into account in system (6). The contagion parameter β could also be chosen depending on space, e.g., maximum in zones which constitute overlaps between domains where diffusion of infective vectors and hosts is minimum and domains where concentration of susceptibles is maximum, ensuring locally a large coexistence time, hence a high contagion rate between these large interacting subpopulations.

7. The feather primordia morphogenesis

The feather primordia morphogenesis is an embryonic process, which allows to well position adult feathers permitting for example to the peacock to do the wheel in order to attract the female (cf. Figure 5).
The reaction-diffusion system corresponding to the feather primordia morphogenesis [Michon *et al.*, 2008] rules 3 variables, the density n of migrant primordial cells and the concentration u (resp. v) of an activator

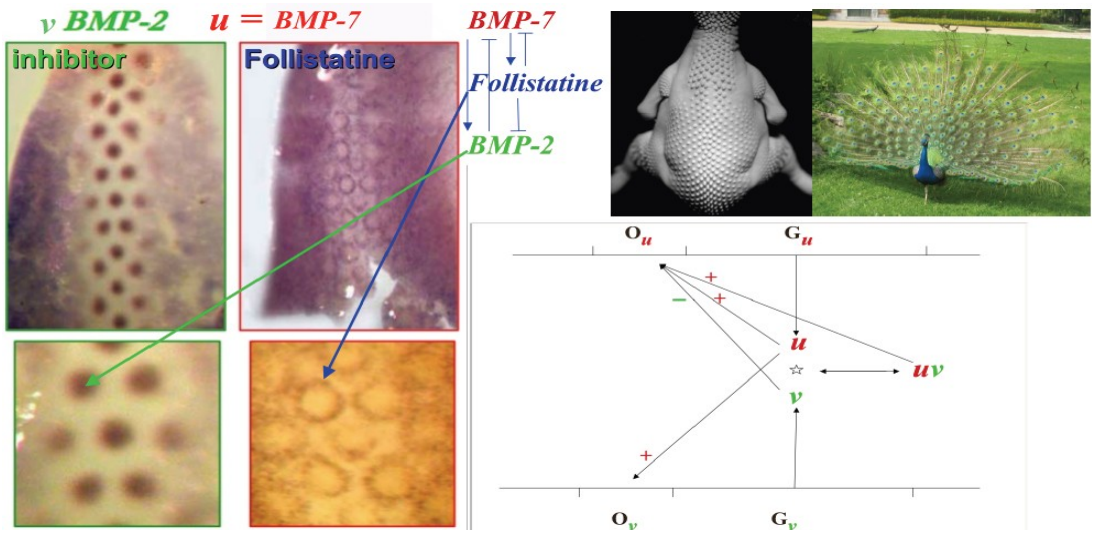

Fig. 5. Feather morphogenesis with identification of an activator u ($BMP-7$), an inhibitor v ($BMP-2$) and a mediator (Follistatine) as morphogens (left) interacting at the genetic level, where G_u (resp. G_v) and O_u (resp. O_v) denote the gene coding for u (resp. v) and its operator (top middle and bottom right) for giving first feathers primordia and after, adult feathers allowing the wheel of feathers in the peacock (top right)

(resp. inhibitor), the $BMP-7$ (resp. $BMP-2$), following the equations:

$$\begin{aligned}
\frac{\partial n}{\partial t} &= -\Box n - \beta \frac{\partial n}{\partial a} + \nabla(\chi n \, \nabla u), \\
\frac{\partial u}{\partial t} &= D_u \, \Delta u + f_0(u,v) - k_u u, \\
\frac{\partial v}{\partial t} &= D_v \, \Delta v + g_0(u,v) - k_v v,
\end{aligned} \tag{10}$$

with $f_0(u,v) = c_1 n u^2/(1+v)$, $g_0(u,v) = c_2 n u^2$, $n(s,1,t) = \int_1^M 2Q\beta C_n(s,a,t) n(s,a,t)\, da$, and also with Neumann boundary conditions. For the sake of simplicity, we will use in the following a simplified equation for n:

$$\frac{\partial n}{\partial t} = D_n \, \Delta n - \nabla(\chi n \nabla u) + bn(1-n) \tag{11}$$

Then it is possible to derive explicitly Turing's instability necessary conditions [Turing, 1952], where u_s (resp. v_s) denotes the stationary concentration of u (resp. v) and f_{0u} (resp. g_{0u}) the first derivative of f_0 (resp. g_0) with respect to u at (u_s, v_s):

(1) $f_{0u} + g_{0u} < 0 \Rightarrow 2c_1 k_v u_s/(k_v + c_2 u_s^2) - k_u - k_v < 0$,
(2) $f_{0u} g_{0v} - f_{0v} g_{0u} > 0 \Rightarrow -2c_1 k_v^2 u_s/(k_v + c_2 u_s^2) + k_u k_v + 2c_1 c_2 k_v^2 u_s^3/(k_v + c_2 u_s^2)^2 > 0 \Rightarrow -2c_1 k_v^3 u_s/(k_v + c_2 u_s^2)^2 + k_u k_v > 0$
(3) $D_u g_{0v} + D_v f_{0u} < 0 \Rightarrow 2D_v c_1 k_v u_s/(k_v + c_2 u_s^2) - D_v k_u - D_u k_v < 0$
(4) $(D_u g_{0v} + D_v f_{0u})^2 > 4 D_u D_v (f_{0u} g_{0v} - f_{0v} g_{0u}) \Rightarrow 2D_v c_1 k_v u_s/(k_v + c_2 u_s^2) - (D_v k_u + D_u k_v) > \left(4 D_u D_v k_u k_v - 8 D_u D_v c_1 k_v^3 u_s/(k_v + c_2 u_s^2)^2\right)^{1/2}$

If $v \ll 1$ and n are near their stationary value, e.g., if D_n, χ and b are large, such as the system reaches rapidly its slow (u,v) manifold, we can decompose the two last equations of (10) in order to get a potential-

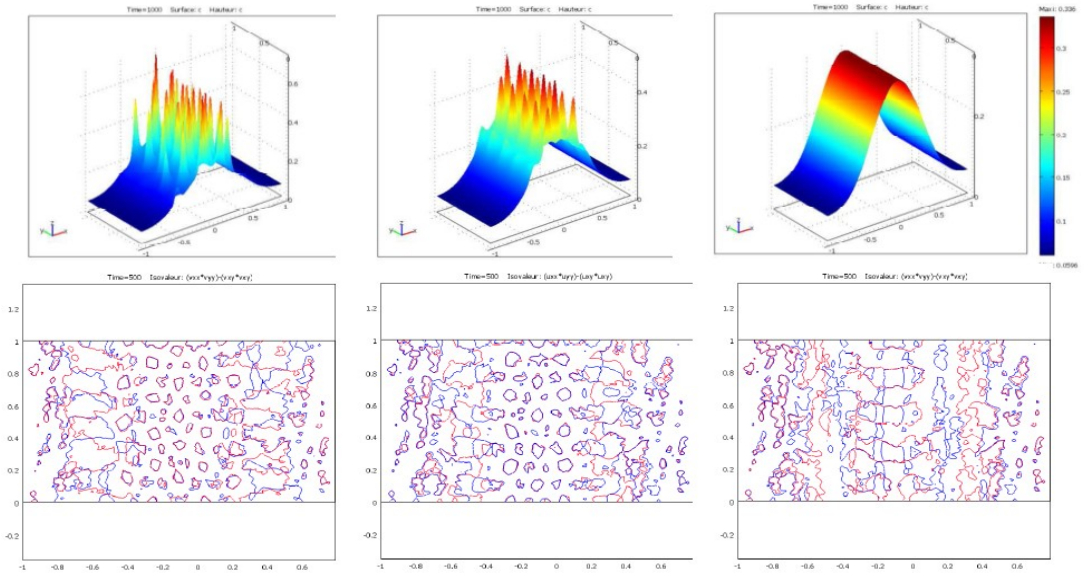

Fig. 6. Coincidence of the null-curvature lines of the u (in red) and v (in blue) concentration surfaces, when D_u/D_v varies from 0.05 (left) to 0.07 (right). For $D_u/D_v = 0.06$ (middle), the coincidence is perfect on the central part of the picture, which corresponds roughly to the experimental value of the diffusion coefficients ratio

Hamiltonian system, with:

$$\begin{aligned}
\frac{\partial u}{\partial t} &= -\frac{\partial P}{\partial u} + \frac{\partial H}{\partial v},\\
\frac{\partial v}{\partial t} &= -\frac{\partial P}{\partial v} - \frac{\partial H}{\partial u},\\
P &= (k_u u^2 + k_v v^2)/2,\\
H &= c_1 n u^2 \ln(1+v) - c_2 n u^3/3.
\end{aligned}$$

Then c_1 and c_2 (resp. k_u and k_v) can be considered as frequency (resp. amplitude) modulating parameters [Demongeot *et al.*, 2007a,b; Forest *et al.*, 2007; Glade *et al.*, 2007] and the synchronizability can be estimated by considering the isochrons landscape of the simplified system [Demongeot & Françoise, 2006].
The last very important parameter is the ratio between the diffusion coefficients D_u/D_v, which is less than 1 as usually in lateral inhibition [Demongeot *et al.*, 2009]: if the ratio is equal to the critical value 0.06, we observe both in experiments (cf. Figure 5) and in simulations (cf. Figure 6) a temporo-spatial synchrony between the effectors u and v. Both experiments and simulations show a coincidence of their remarkable Gaussian lines, i.e. the projections of the null-curvature lines on the u and v concentration surfaces, defined by the following equations expressing the vanishing of the mean Gaussian curvature:

$$C_u(x,y,t) = \frac{\partial^2 u}{\partial x^2}\frac{\partial^2 u}{\partial y^2} - \left(\frac{\partial^2 u}{\partial x \partial y}\right)^2 = 0,$$

$$C_v(x,y,t) = \frac{\partial^2 v}{\partial x^2}\frac{\partial^2 v}{\partial y^2} - \left(\frac{\partial^2 v}{\partial x \partial y}\right)^2 = 0.$$

These two remarkable lines for the effectors u and v coincide for the critical value of $D_u/D_v = 0.06$ (cf. Figure 6). The $2D$ projections of these lines form front waves moving in the same direction as the fronts of the concentration contour lines, and where they coincide, the diffusion term vanishes and u and v are susceptible to form at this location an assemblage like the phospho-lipo-proteic plasmic membrane or the

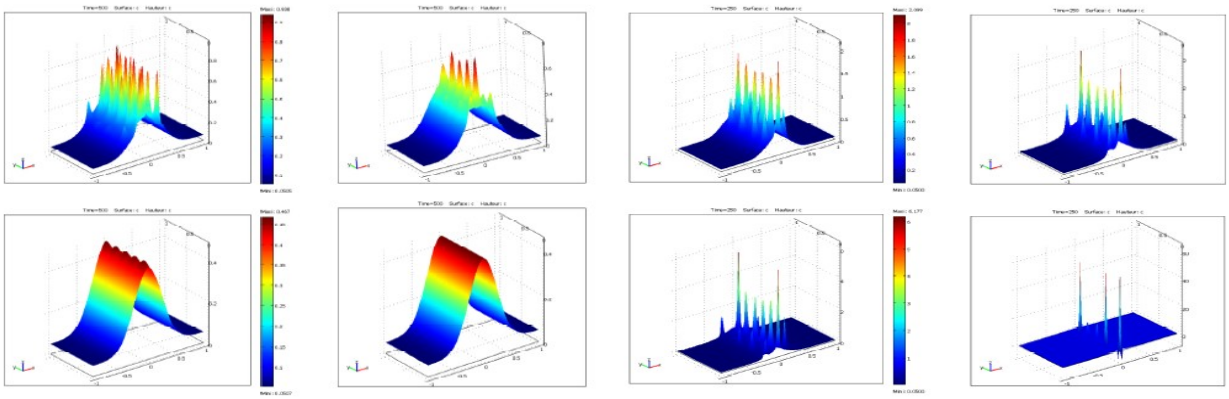

Fig. 7. On the left: diminishing k_v (from 35 to 0 with step of 5) causes the decrease of the feather number and amplitude. On the right: diminishing c_2 (from 4500 to 1200 with step 1100) causes feather motifs disparition and diffusion wins over reaction

inner mitochondrial membrane [Demongeot *et al.*, 2007c]. The coexistence at this common least diffusion location of migrant cells n as well as morphogens u and v permits indeed to build an anatomic boundary for the future feathers, avoiding chemical reactions between these components, which change their physical nature and involve thermic fluctuations (hence no zero diffusion). These phenomena are summarized on Figure 6 which shows the coincidence (or the spatial synchrony) between the remarkable lines in $2D$, suggesting that this mechanism can be met in many circumstances of formation of an anatomic boundary: for example, in [Demongeot *et al.*, 2007c], a lateral inhibition mechanism is also used to show a spatial synchrony between transmembrane proteins (the ATPase and the Translocase) allowing the realization of a variational principle, which maximizes the mitochondrial ATP production and minimizes the mean free path of adenylates inside the mitochondrion, by favouring the spatial vicinity between the ATPase and Translocase sites inside the inner mitochondrial membrane. Many other parameters like c_2 and k_v are critical for the occurrence of feathers (cf. Figure 7).

8. The gastrulation process

The gastrulation process is critical for a living organism, because it initiates the construction of the digestive tube, just before the neural chord (cf. Figures 8 and 9). Many experimental observations show that invagination preceding tube cylindrization starts on the two embryo extremities and propagates until its middle part (cf. Figure 10 D), where occurs a high concentration of myosin in bottle cells (yellow on Figure 10 E). In these cells, apical constriction occurs when actomyosin contractility folds the cell membrane to reduce the apical surface area. By considering a $3D$ mesh representing the terminal region where curvature changes, we can simulate "in silico" the phenomenon by only taking into account the contractility in the central cells of the mesh due to a local excess of mysosin diffusing from a random fluctuation in the central embryonic part.

A gastrulation model needs to account for 4 mechanisms, allowing realistic simulations:

(1) change (due to random fluctuations) in concentration of metabolites critical for cell shape, like myosin, actin, tubulin or of the substrates (notably ATP, GTP) and enzymes ruling adenylate and guanylate pools (mainly ADenylate Kinase or ADK, Guanylate Kinase or GK and Nucleoside-Diphosphate Kinase or NDK) required for their polymerization. The cell shape change into a truncated pyramid (or bottle, or flask) shape is achieved in the apical portion of the cell which constricts

(2) diffusion of critical metabolites provoking locally the bottle cell differentiation (in region 1 on Figure 11)

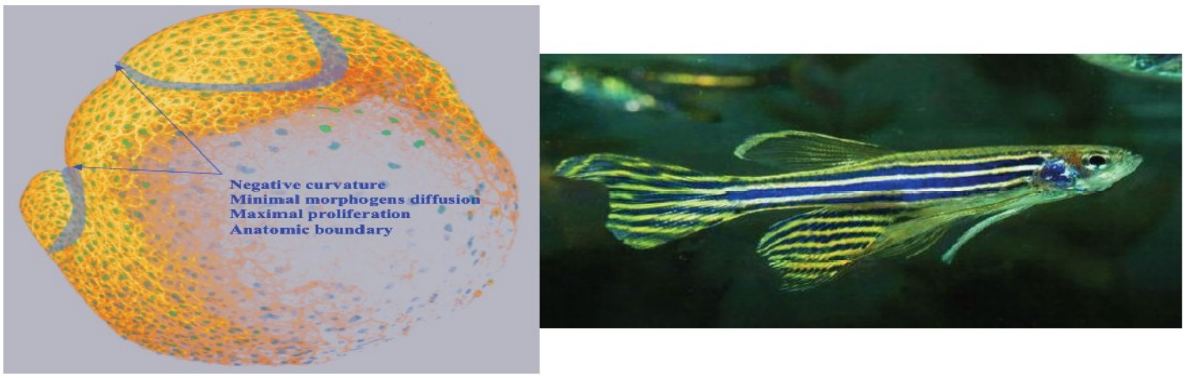

Fig. 8. In grey, eyes, gills and gastrula cavity anatomic frontiers in Zebra fish embryo (left, [Zanella *et al.*, 2010], corresponding to negative curvature, maximal proliferation and minimal morphogen diffusion domains. Adult animal (right)

(3) cell contraction from the apical cell surface (cf. 2 on Figure 11) and centrosome displacement in the cell depth at the cell extremities due to the elastic forces balance during the first invagination stage of the gastrulation (3 on Figure 11), which is purely mechanical without proliferation
(4) cell cycle arrest for bottle cells [Kurth, 2005] and after, proliferation at the end of gastrulation, consolidating the tube formation (4 on Figure 11). For example, the onset of gastrulation in rodents is associated with the start of bottle cell differentiation within the embryo proper and after, with a dramatic increase in the rate of growth and proliferation, the cell cycle time being 7 to 7.5 hours in ectoderm and mesoderm, but 3 to 3.5 hours in the cells of the primitive streak, whose total cell cycle time is reduced by shortening S and $G2$, as well as $G1$ in contrast to cells later in development, where the cell cycle duration is modulated by varying the $G1$ length [Mac Auley *et al.*, 1993].

The gastrulation model formalizes the mechanisms causing the mechanical perturbations due to the first bottle cell differentiation (cell 2 in blue on Figure 11): after the apical constriction of the upper cells (cf. Figures 10 and 11) and myosin diffusion, each cell evolves with its walls following the Newton law: the sum of exerted forces is equal to the acceleration of the wall in the resultant direction (the mass of a wall being equal to 1), and each cell is submitted to forces related to internal and external pressures (created by elastic forces applied from the centrosome to the cells extremities in Figure 10 bottom), plus contact forces imposed by neighbour cells. Each force is orthogonally applied to the concerned cell wall and is proportional to its length, coefficients being either the pressure or the cadherins concentration. The updating of each cell force balance is sequential: when a cell moves, it takes its neighbours with itself. These movements cause variations of cells areas: we suppose that growth occurs where the forces are high and that cells are incompressible. After a radial division due to a small nutritive surface/volume ratio of the bottle cells (following the Thom's law, described in [Forest & Demongeot, 2004, 2008; Forest *et al.*, 2004, 2006], we suppose that the growth in $G1$ following the mitosis increases this ratio, ensuring a convenient nutrition. Cells are often shaped by requirements of cell surface S over volume V ratio (S/V) and namely intestinal cells have tendency to increase the area through which nutrients are absorbed [Stanek, 1983; Miller & Levine, 2002]. Ratio S/V decreases when invagination occurs (cf. Figure 9 bottom), especially if actomyosin fibers are orthogonal to microtubules [Silverman-Gavrila *et al.*, 2008], depolymerization reducing the extent of the apical constriction [Lee & Harland, 2010]. Forces exerted on walls push centrosome and nucleus to move in the cell depth at the level of the first curved distal parts of the embryo (cf. Figures 9 & 10) in agreement with experiments [Leptin & Grünewald, 1990], due to the location of the elastic forces application points supposed to be the same on neighbour walls, located at the cadherin and myosin-membrane-attached

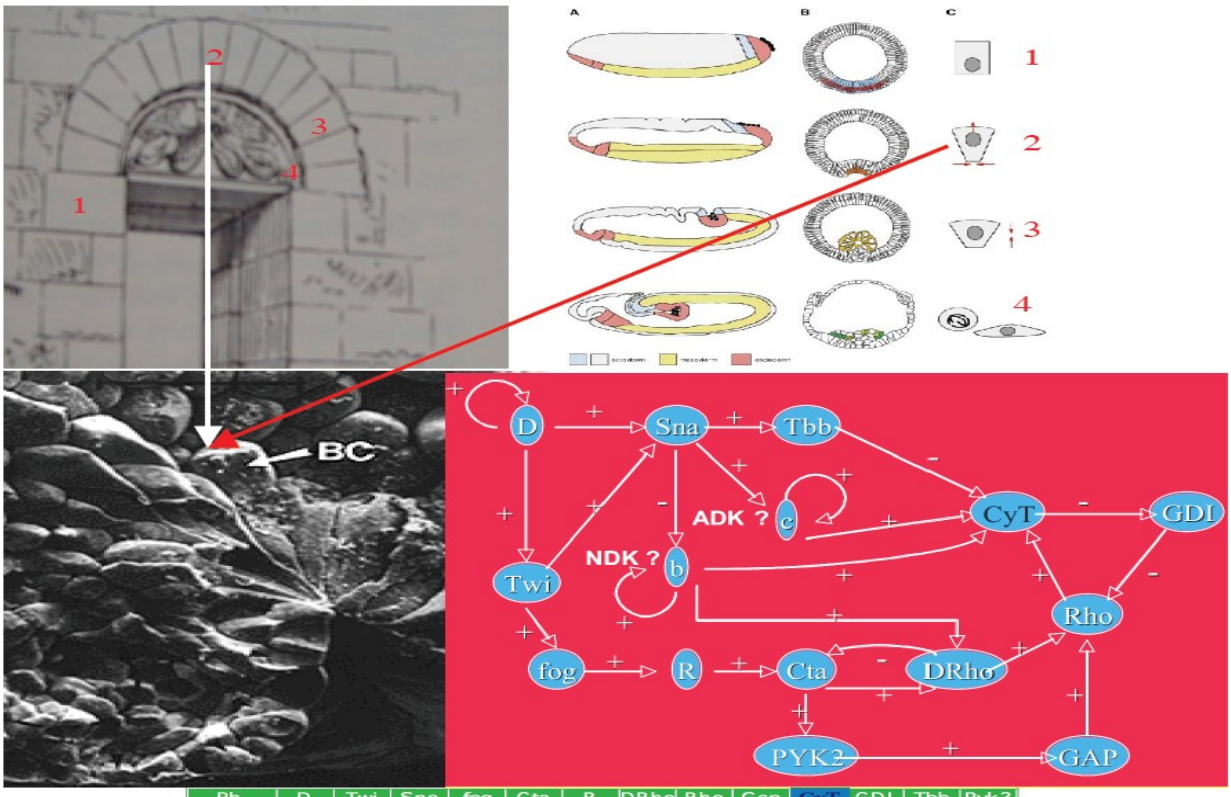

Ph.	D	Twi	Sna	fog	Cta	R	DRho	Rho	Gap	CyT	GDI	Tbb	Pyk2
	0	0	0	0	0	0	1	0	0	0	1	1	0
	1	1	1	1	1	1	1	1	1	1	0	0	1
	1	1	1	1	1	1	1	1	1	1	0	0	1
	1	1	1	1	1	1	1	1	1	1	0	0	1

Fig. 9. Building gastrulation cavity with invagination first phase showing 4 types of cells: 1) the exothelial, 2) the bottle (BC on middle left, arch "keystone"), 3) the trapezoidal and 4) the endothelial (top). Genetic network ruling the gastrulation, with only 2 fixed point attractors, if genes b and c vanish (middle right and bottom)

sites [Inoue, 1995; Angst *et al.*, 2001; Laevsky & Knecht, 2003; Hanson *et al.*, 2007]. Expression of genes like Rho (cf. Figure 9) ruling enzymes and carrier proteins needed for controlling metabolites critical for cell shaping [Chisholm, 2006] depends on a genetic regulatory network described in [Leptin, 1999; Demongeot *et al.*, 2003; Aracena *et al.*, 2006]. Figure 9 shows the minimal architecture having 4 attractors corresponding to the 4 cell types needed for achieving the digestive tube.

The domains of minimal diffusion of myosin are shown in yellow on Figure 9 and are located on the frontiers of the invagination (zones of zero-curvature). The link between these domains and the anatomic boundaries have to be confirmed in further $3D$ microscopic studies by comparing the null-curvature maps of the embryo, the zero-diffusion domains of the critical metabolites and the maximal proliferation zones. We conjecture in concluding these two short studies about feather morphogenesis and gastrulation that the zero-diffusion sets could be good candidates for ensuring locally the coexistence, and after the auto-assemblage of the components (carrier, receptor and attachment proteins as well as phospho-lipids) of cell interfaces between two tissues needed for separating organs functionnally specified by differentiated cells. In the zero-diffusion zones indeed the effect of the temperature on the diffusion is minimum, because the viscosity (inverse of

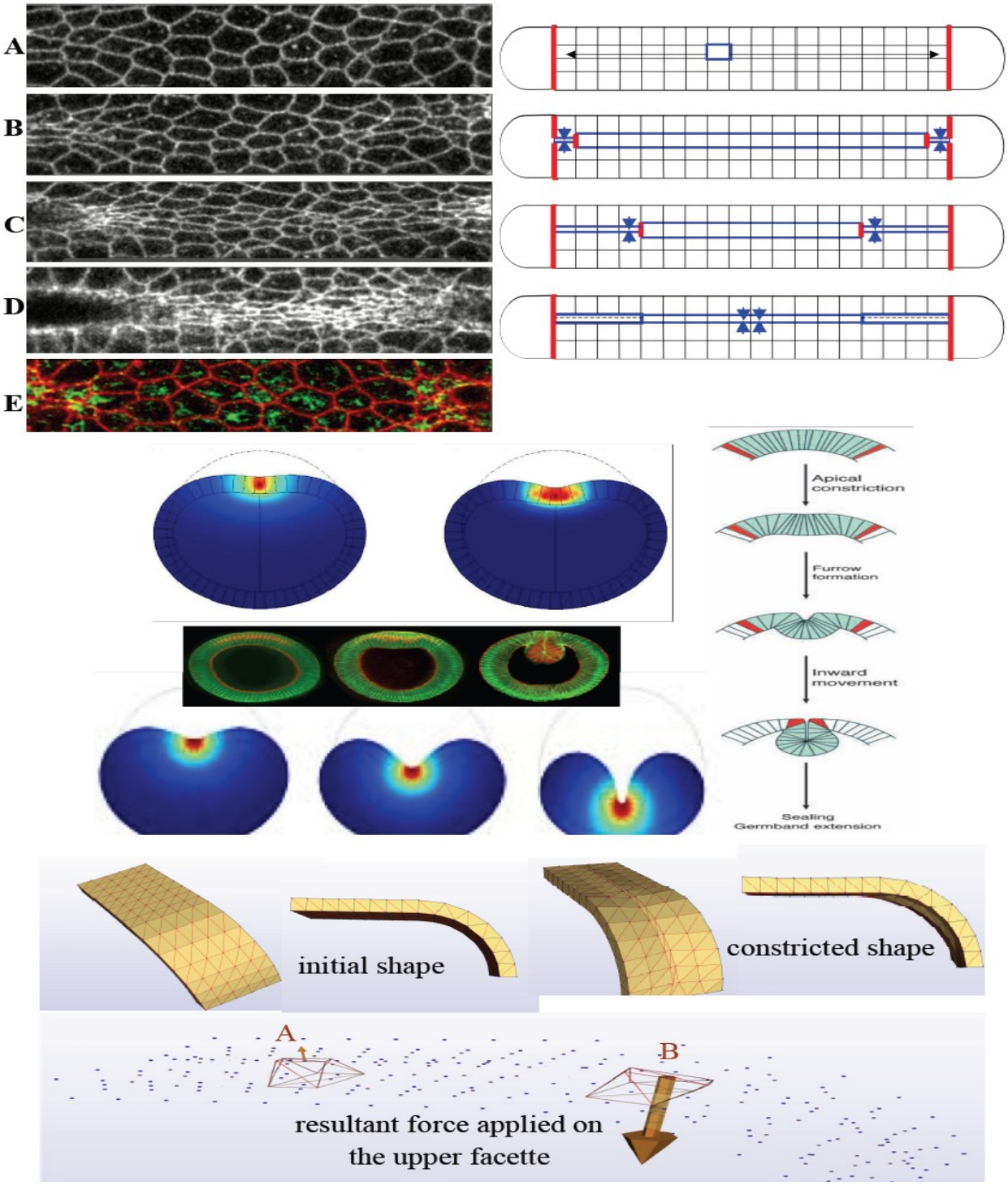

Fig. 10. Progressive invagination due to the first bottle cell differentiation in gastrulation process: experimental data (top left, from http://www.molbio1.princeton.edu/wieschaus/); tentative mechanism of propagation of the random myosin fluctuation (in blue, top right); model with myosin diffusion (in red) and cell contraction, yellow color indicating the zones of minimal diffusion (middle left) with explanation of the inward movement (middle right) and central mesh contraction showing the terminal invagination in axonometric and profile views, with calculation of forces exerted by the elastic constraints propagation on a central and distal cell, located respectively on the cylindric (A) and curved terminal (B) parts of the embryo (bottom)

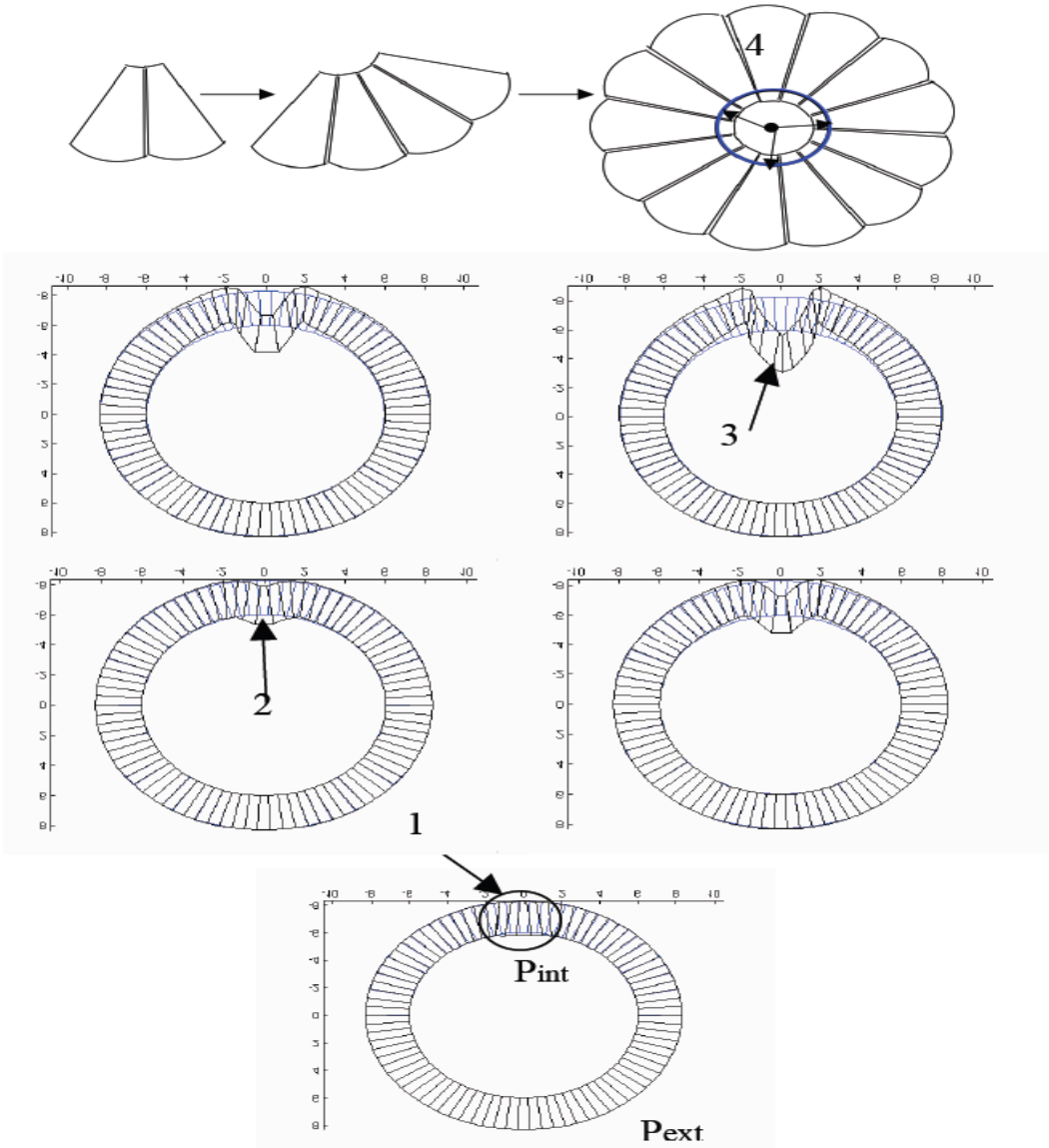

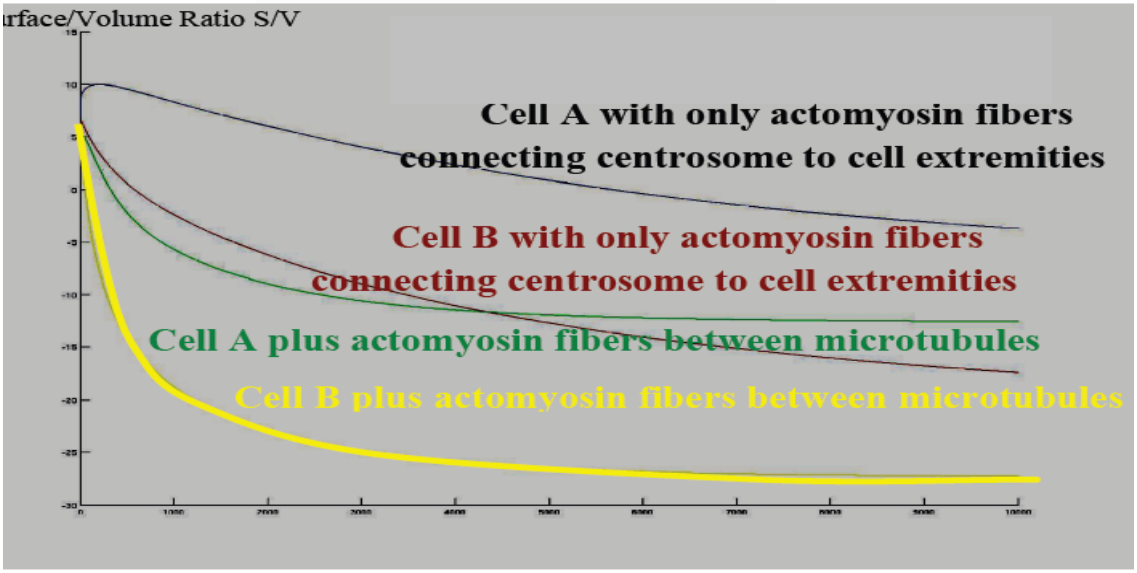

Fig. 11. Top: First steps of the gastrulation with 1) diffusion of constriction metabolites from the first bottle cells (in blue), 2) occurrence of the invagination from the initial bottle cell and 3) proliferation of bottle cells, before 4) closing and enlarging the tube. Bottom: Curves showing the cell surface S over cell volume V ratio (S/V) depending on the mode of attachment of the myosin fibers inside the cells A and B of Figure 10

the diffusion coefficient D) is proportional to $\exp(E/kT)$, where E is an activation energy, T the absolute temperature and k the Boltzmann's constant. We can also notice that if the concentration front wave is Gaussian, the zero-diffusion zone corresponds to the domain where the partial de Donder affinity $\ln(u)$, where u is the concentration of the diffusing substance [Dutt, 2000], does not vary, after reaching the reaction equilibrium, in the case where the reaction has a fast dynamics with respect to a slow diffusion:

$$\frac{\partial \ln(u)}{\partial t} = \frac{1}{u}\frac{\partial u}{\partial t} = \frac{D\,\Delta u}{u}$$

If we authorize the value of $D\Delta_u/u$ to be sufficiently small, that corresponds also to the domain where the diffusion of u is minimum and its concentration maximum. If the corresponding value of u minimizes a chemical potential from which the reaction velocity derives, like in n-switches involved in morphogenetic processes [Cinquin & Demongeot, 2002a,b], then the zero-diffusion domains, in the case where they coincide for several constituents (e.g., of a membrane or aponeurosis), correspond to a local constancy of their concentrations favouring their interactions in order to build the auto-assemblage the least sensitive to the thermal fluctuations.

9. Conclusion

We have considered firstly in this paper some natural extensions of the classical Ross-McKendrick-Mac Donald approaches, in order to account for demographic and spatial dependencies of the variables involved in an infection process. One example has been presented, concerning the Black Death spread in Europe during the middle-age, which shows the interest of introducing space and biological age into the classical equations. In the future, other infectious diseases (like Sexually Transmitted Diseases) could be treated with the same approach showing the importance of the demography (the sexual relationships depending on the age of the partners) and of the socio-geography (conditioning the sexual behavior). Based on the knowledge of the new aerial routes [Khan *et al.*, 2009], epidemics modelling will be also revisited in a short future for predicting new pandemics, with a viscosity minimal on the aerial routes. A second type of spatial dependency in a reaction-diffusion process occurs in the morphogenesis modelling: like for the epidemics, both age and spatial diffusion can explain the occurrence of spatial patterns, e.g., in the cases of feather morphogenesis and gastrulation.
In both epidemics and morphogenesis models, further studies have to be done in order to definitely emphasize and make more precise the functional role of the zero-diffusion domains, in which chemical or infectious agents coexist and interact.

10. Acknowledgements

We are very indebted to L. Forest for his invaluable contribution to models and simulations, and for his unforgettable friendship, and to N. Peyriéras for showing the direction of a new experimental research through the EEC project "Bioemergences". The present work has been partially granted by the EEC VPH (Virtual Physiological Human) Network of Excellence.

References

Abbas, L., Demongeot, J. & Glade, N. [2009] "Synchrony in Reaction-diffusion models of morphogenesis: applications to curvature-dependent proliferation and zero-diffusion front waves", *Phil. Trans. Royal Soc. A.* **367**, 4829-4862.

d'Alembert, J. [1761] *Opuscules Mathématiques* (David, Paris).

Angst, B. D., Marcozzi, C. & Magee, A. I. [2001] "The cadherin superfamily diversity in form and function", *J. Cell Biol.* **117**, 629-641

Aracena, J., González M., Zuñiga, A., Mendez, M. A. & Cambiazo, V. [2006] "Regulatory network for cell shape changes during Drosophila ventral furrow formation", *J. Theor. Biol.* **239**, 49-62.

Barry, S. & Gualde, N. [2006] "The Biggest Epidemics of History", *L'Histoire* **310**, 38-49.

de Baux, P. [1766] *Réflexions présentées à la Faculté de Médecine de Paris sur le rapport de six des douze commissaires nommés par ladite Faculté (Favet, Marseille).*

Benedictow, O. J. [2004] *The Black Death 1346-1353: The Complete History*, Boydell Press, Woodbridge, UK.

Bernoulli, D. [1760] *Essai d'une nouvelle analyse de la mortalité causée par la petite vérole, et des advantages de l'inoculation pour la prévenir.* Acad. Roy. Sci., Paris.

Chisholm, A. D. [2006] "Gastrulation: Wnts Signal Constriction", *Current Biology* **16**, 874-876.

Cinquin, O. & Demongeot, J. [2002a] "Positive and negative feedback : striking a balance between necessary antagonists", *J. Theor. Biol.* **216**, 229-241.

Cinquin, O. & Demongeot, J. [2002b] "Positive and negative feedback: mending the ways of sloppy systems", *Comptes Rendus Biologies* **325**, 1085-1095.

Crauste, F., Hbid, M. L. & Kacha, A. [2008] "A delay reaction-diffusion model of the dynamics of botulinum in fish", *Maths Biosciences* **216**, 17-29.

Demongeot, J. [1983]. "Coupling of Markov processes and Holley's inequalities for Gibbs measures", *Proc. IXth Prague Conference on Information Theory, Statistical Decision Functions and Random Processes, (Academia, Prague), pp.* 183-189.

Demongeot, J. & Fricot [1986] J. "Random fields and renewal potentials", *NATO ASI Serie F* **20**, 71-84.

Demongeot, J., Aracena, J., Thuderoz, F. Baum, T. P. & Cohen, O. [2003] "Genetic regulation networks: circuits, regulons and attractors", *Comptes Rendus Biologies* **326**, 171-188.

Demongeot, J. & Françoise, J. P. [2006] "Approximation for limit cycles and their isochrons", *Comptes Rendus Biologies* **329**, 967-970.

Demongeot, J., Glade, N. & Forest, L. [2007a] "Liénard systems and potential-Hamiltonian decomposition. I Methodology", *Comptes Rendus Mathématique* **344**, 121-126.

Demongeot, J., Glade, N. & Forest, L. [2007b] "Liénard systems and potential-Hamiltonian decomposition. II Algorithm", *Comptes Rendus Mathématique* **344**, 191-194.

Demongeot, J., Glade, N., Hansen, O. & Moreira, A. [2007c] "An open issue: the inner mitochondrial membrane (IMM) as a free boundary problem", *Biochimie* **89**, 1049-1057.

Demongeot, J. [2009] "Biological boundaries and biological age", *Acta Biotheoretica* **57**, 397-419.

Demongeot, J., Fouquet, Y., Tayyab, M. & Vuillerme, N. [2009] "Understanding Physiological & Degenerative Natural Vision Mechanisms to Define Robust Contrast and Segmentation Operators", *PLoS ONE 4, e6010.*

Dietz, K. & Heesterbeek, J. A. P. [2000] "Bernoulli was ahead of modern epidemiology", *Nature* **408**, 513.

Dietz, K & Heesterbeek, J. A. P. [2002] "Daniel Bernoullis epidemiological model revisited", *Math. Biosci.* **180**, 121.

Dutt, A. K. [2000] "Non-equilibrium thermodynamics of a model bistable chemical system", *Chemical Physics Letters* **322**, 73-77.

Fisher, R. A. [1937] "The wave of advance of advantageous genes", *Ann. Eugenics* **7**, 353369.

Forest, L. & Demongeot, J. [2004] " Cellular modelling of secondary radial growth in conifer trees: application to Pinus radiata", *Bull. Math. Biol.* **68**, 753-784.

Forest, L., San Martin, J., Padilla, F., Chassat, F., Giroud, F. & Demongeot, J. [2004] "Morphogenetic processes: application to cambial growth dynamics", *Acta Biotheoretica* **52**, 415-438.

Forest, L., Martinez, S., Padilla, F., Demongeot, J. & San Martin, J. [2006] "Modelling of auxin transport affected by gravity and differential radial growth", *J. Theor. Biol.* **241**, 241-251.

Forest, L., Glade, N. & Demongeot, J. [2007] "Liénard systems and potential-Hamiltonian decomposition. Applications", *C. R. Acad. Sci. Biologies* **330**, 97-106.

Forest, L. & Demongeot, J. [2008] "A general formalism for tissue morphogenesis based on cellular dynamics and control system interactions", *Acta Biotheoretica* **56**, 51-74.

Gaudart, J., Giorgi, R., Poudiougou, B., Ranque, S., Doumbo O. & Demongeot, J. [2007] "Spatial cluster detection: principle and application of different general methods", *Rev. Ep. Santé Pub.* **55**, 297-306.

Gaudart, J. Touré, O., Dessay, N., Dicko, A. L., Ranque, S., Forest, L., Demongeot, J. & Doumbo, O. K. [2009] "Modelling malaria incidence with environmental dependency in a locality of Sudanese savannah area, Mali", *Malaria J.* **8**, 61.

Gaudart, J., Ghassani, M., Mintsa, J., Waku, J., Rachdi, M., Doumbo, O. K. & Demongeot, J. [2010] "Demographic and spatial factors as causes of an epidemic spread, the copule approach. Application

to retro-prediction of the Black Death of 1346", *IEEE AINA'2010 (IEEE Press, Piscataway), pp.* 751-758.

Glade, N., Forest, L. & Demongeot, J. [2007] "Liénard systems and potential-Hamiltonian decomposition. III Applications in biology", *Comptes Rendus Mathématique* **344**, 253-258.

Hanson, P. I., Roth, R., Lin, Y. & Heuser, J.E. [2007] "Plasma membrane deformation by circular arrays of ESCRT-III protein filaments", *J. Cell Biol.* **180**, 389- 402.

Horie, M., Honda, T., Suzuki, Y., Kobayashi, Y., Daito, T. Oshida, T., Ikuta, K., Jern, P., Gojobori, T., Coffin, J. M. & Tomonaga, K. [2010] "Endogeneous non-retroviral RNA virus elements in mammalian genomes", *Nature* **463**, 84-88.

Inoue, S. [1995] "Possible continuity of subplasmalemmal cytoplasmic network with basement membrane cord network: ultrastructural study", *J. Cell Biol.* **108**, 1971-1976.

Kermack, W. O. & McKendrick, A. G. [1932] "Contributions to the Mathematical Theory of Epidemics. II. The Problem of Endemicity", *Proceedings of the Royal Society of London Series A* **138**, 55-83.

Kermack, W. O. & McKendrick, A. G. [1933] "Contributions to the Mathematical Theory of Epidemics. III. Further Studies of the Problem of Endemicity", *Proceedings of the Royal Society of London Series A* **141**, 94-122.

Khan, K., Arino, J., Hu, W., Raposo, J., Sears, J., Calderon, F., Heidebrecht, C., Macdonald, M., Liauw, J., Chan, A. & Gardam, M. [2009] "Spread of a novel Influenza A (H1N1) virus via global airline transportation", *New England Journal of Medicine* **361**, 212-214.

Kurth, T. [2005] " A cell cycle arrest is necessary for bottle cell formation in the early Xenopus gastrula: integrating cell shape change, local mitotic control and mesodermal patterning", *Mech. Dev.* **122**, 1251-1265.

Laevsky, G. & Knecht, D. A. [2003] "Cross-linking of actin filaments by myosin II is a major contributor to cortical integrity and cell motility in restrictive environments", *J. Cell Biol.* **116**, 3761-3770.

Lambert, J. H. [1972] *Beiträge zum Gebrauche der Mathematik und deren Anwendung*, Dritter Theil, Berlin.

Lee, J. & Harland, R. M. [2010] "Endocytosis is required for efficient apical constriction during Xenopus Gastrulation", *Current Biology* **20**, 253-258.

L'épine, G. J. [1764] *Rapport de six des douze commissaires nommés par la Faculté de Médecine à Paris, pour examiner, discuter les avantages et les inconvénients de l'inoculation de la petite vérole*, Faculté de Médecine, Paris.

Leptin, M. & Grünewald, B. [1990] " Cell shape changes during gastrulation in Drosophila", *Development* **110**, 73-84.

Leptin, M. [1999] "Gastrulation in Drosophila: the logic and the cellular mechanisms", *Embo J.* **18**, 3187-3192.

Leslie, P. H. [1945] "On the use of matrices in certain population mathematics", *Biometrika* **33**, 183-212.

Mac Auley, A., Werb, Z. & Mirkes, P. E. [1993] "Characterization of the unusually rapid cell cycles during rat gastrulation", *Development* **117**, 873-883.

Mac Donald, G. [1957] *The epidemiology and control of malaria*, Oxford University Press, Oxford.

McKendrick, A. G. [1925] "Applications of mathematics to medical problems", *Proc. Edinburgh Mathematical Society* **44**, 1-34.

May, N. [1770] *Impartial remarks on the Suttonian method of inoculation*, Tilley, London.

May, R. M. & Anderson, R. M. [1984] "Spatial heterogeneity and the design of immunization programs", *Math. Biosci.* **72**, 83111.

Michon, F., Forest, L., Collomb, E., Demongeot, J. & Dhouailly, D. [2008] "BMP-2 and BMP-7 play antagonistic roles in feather induction", *Development* **135**, 2797-2805.

Mendez, V., Fort, J., Rotstein, H. G. & Fedotov, S. [2003] "Speed of reaction-diffusion fronts in spatially heterogeneous media", *Phys. Rev. E* **68**, 041105.

Miller, K.R & Levine, J. [2002] *Biology*, Prentice Hall, Upper Saddle River, New Jersey, pp. 242-243.

Mocellin-Spicuzza, G. [2002] Chroniques d'une abbaye au Moyen-Age. Guérir l'âme et le corps. Ed. Musée, Saint-Antoine l'Abbaye.

Murray, J. A. [1763] *Fata insitionis variolarum in Suecia,* University of Göttingen, Göttingen.

Murray, J. D. [2003] *Mathematical Biology: II. Spatial Models and Biomedical Applications*, Springer, Berlin.

Ross, R. [1916] "An Application of the Theory of Probabilities to the Study of a priori Pathometry. Part I", *Proceedings of the Royal Society of London Series A* **92**, 204-230.

Silverman-Gavrila, R. V., Hales, K. G. & Wilde, A. [2008] "Anillin-mediated Targeting of Peanut to Pseudocleavage Furrows Is Regulated by the GTPase Ran", *Mol. Biol. Cell.* **19**, 37353744.

Sprengel, K. [1815] "Histoire de l'inoculation de la petite vérole", *Histoire de la Médecine (Deterville, Paris)*, pp. 33-81.

Stanek, Jr., J. A. [1983] "Why don't cells grow larger?", *American Biology Teacher* **45**, 393-395.

Turing, A. M. [1952] "The Chemical Basis of Morphogenesis", *Philosophical Transactions of the Royal Society of London* **B 237**, 37-72.

Trembley, J. [1796] *Recherches sur la mortalité de la petite vérole*, Mém. Acad. Roy. Sci., Paris.

Usher, M. B. [1969] "A Matrix Model for Forest Management", *Biometrics* **25**, 309-315.

WHO [1999] "La peste humaine en 1997", *Relevé Epidémiologique Hebdomadaire OMS* **74**, 340-344.

Zanella, C., Campana, M., Rizzi, B., Melani, C., Sanguinetti, G., Bourgine, P., Mikula, K., Peyrieras, N. & Sarti, A. [2010] "Cells segmentation from 3-D confocal images of early zebrafish embryogenesis", *IEEE Trans Image Process.* **19**, 770-781.

Zeeman, E. C. [1993] "Controversy in science: on the ideas of Daniel Bernoulli and René Thom", *Nieuw Arch. Wisk.* **11**, 257.

Zhang, S. Y., Yu, L. & Daszak, P. [2008] "EcoHealth and the Black Death in the Year of the Rat", *Ecohealth* **5**, 99-100.